

Nonlinear Stable Inversion-Based Output Tracking Control for a Spherical Inverted Pendulum

Guangyu Liu, Dragan Nešić, and Iven Mareels*

Department of Electrical & Electronic Engineering,
The University of Melbourne, Parkville, 3010, Victoria, Australia.

(v1.1 released January 2006)

We design an exact output tracking control law for a four degree of freedom spherical inverted pendulum based on the nonlinear stable inversion tool proposed by Devasia, Chen and Paden. The pendulum is a slim cylindrical beam attached to a horizontal plane via a universal joint; the joint is free to move in the plane under the influence of a planar force. The upright position is an unstable equilibrium of the uncontrolled system because of gravity. The objective is to design a controller so that the pendulum can be steered to track some smooth desired translational trajectories while keeping the pendulum tightly around the upright position. The design proceeds in three steps: 1) identification of the internal dynamics; 2) feedforward control design for achievable trajectories; 3) feedback design to stabilize the achievable trajectories. The computer simulations show that the proposed controller can deliver excellent tracking performance.

Key words: a spherical inverted pendulum, stable inversion, output tracking, nonlinear,

1 Introduction

The spherical inverted pendulum is a cylindrical beam attached to a horizontal plane via a universal joint (see Figure 1). The pendulum's universal joint is free to move in the horizontal plane, under the influence of a planar force. Gravity acts on the beam making the downward position the naturally stable position. The control objective considered here is to use the planar force to drive the inverted pendulum in such a way that the universal joint of the pendulum tracks some smooth desired trajectory $(x_d(t), y_d(t))$ in the horizontal plane of an inertial reference frame whilst the state is bounded such that the pendulum is kept upwards.

The spherical inverted pendulum is commonly found in control laboratories. Its model resembles several other systems found in robotics and aerospace engineering. For instance, the spherical inverted pendulum is an abstraction for a vector thrust controlled body hovering at a given altitude.

The spherical inverted pendulum is a nonlinear, non-minimum phase, underactuated and MIMO system. The modeling of a simplified spherical inverted pendulum (i.e., a bob with mass m supported by a massless beam) on a cart was considered in Olfati-Saber (2001); Bloch *et al.* (2000, 2001). The modeling for a slim cylindrical beam—a rigid body (see Figure 1) was given explicitly in Liu *et al.* (2005) and Liu *et al.* respectively used the generalized coordinates suggested in Bloch *et al.* (2000) and Olfati-Saber (2001). Non-local stabilization was investigated using the method of controlled Lagrangians (see Bloch *et al.* (2000, 2001)). A full “global” stabilization¹ was first solved explicitly by designing a high and low gain controller in Liu *et al.* (see also the conference version Liu *et al.* (2005)) which incorporates several approaches but essentially exploits the forwarding tool proposed by Teel (1996). To the best of our knowledge, there is no trajectory tracking control for this system in the literature to date. Here, we propose a controller that

*Corresponding author. Email: {g.liu, d.nesic, i.mareels}@ee.unimelb.edu.au

¹“Global” stabilisation denotes that the initial angles of the pendulum are in the upper hemisphere with arbitrary translational positions and arbitrary velocities. In other words, we do not consider “swing up” of the pendulum.

deals with nonlinear output tracking for the spherical inverted pendulum using the technique introduced by Devasia *et al.* (1996). Our work here builds and extends our “global” stabilization work Liu *et al.* in the direction of tracking control.

System inversion can be used to find the input which achieves exact output-tracking of a desired output trajectory (see Hirschorn (1995)). A problem with the standard inversion technique in Hirschorn (1995) is that the computed inverse input tends to be unbounded for system with nonlinear non-minimum phase internal dynamics. This problem can be solved by using a stable inversion approach in Devasia *et al.* (1996) (see Hunt *et al.* (1996) for the linear counterpart). The Byrnes-Isidori regulator (see Isidori (1995)) can be applied to any trajectory generated by a given exosystem, but it requires the nontrivial solution of a set of partial differential algebraic equations. The stable inversion technique trades this requirement for a specific trajectory (rather than any one of a family) without exosystem. The research in inversion theory has been motivated by applied and experimental research problems, for example, the development of optimal inversion methods to account for actuator saturation and bandwidth limitations (see Dewey *et al.* (1998)), for the stable inversion under plant uncertainty (see Devasia (2002)).

A stable inversion-based output tracking control law for a nonlinear non-minimum phase system comprises of two parts: a feedforward control and a feedback control. The bounded feedforward control (non-causal) is found through stable inversion. It plays the role of “guidance”. The feedback control acts as regulator to minimize tracking errors and deals with disturbances. The bounded (desired) trajectories of the internal dynamics are also found through the stable inversion. The feedback gains are determined by applying static feedback design tools. To find the feedforward input and the state trajectory, the desired output trajectory over the whole horizon must be specified in advance. Practically, one can use a finite preview stable inversion such that finite preview information is used to achieve small tracking errors but not asymptotically stable tracking (see Zou and Devasia (2004)).

The stable inversion technique has been successfully applied to a number of systems such as flexible structures and manipulators (see Yim and Singh (1997)), aircraft systems (see Zou and Devasia (2004)), high precision positioning of piezoactuator (see Croft *et al.* (2001)) and the inverted pendulum with two carts (see Devasia (1999)).

This paper designs an exact output tracking controller for the spherical inverted pendulum by applying nonlinear inversion approach proposed in Devasia *et al.* (1996). We proceed with the design in three steps: 1) first we determine the internal dynamics; 2) for some smooth output profiles which are achievable by stable inversion, the feedforward action is derived, yielding the desired state trajectories and the desired input; 3) the feedback gains are designed using a LQR approach.

The paper is organized as follows. In Section II, the stable inversion technique in Devasia *et al.* (1996) is reviewed. In Section III, the modeling for the pendulum, a slim cylindrical beam, is derived by using the coordinates suggested in Bloch *et al.* (2001) and the tracking problem is formulated. In Section IV, an output tracking controller is proposed for the pendulum to asymptotically track some smooth desired output trajectories which are achievable by the stable inversion technique. In Section IV, the simulation results is presented for a specific output profile. Final observations are given in Section V.

2 Preliminaries

2.1 Notations

We use $(x_1, x_2) \triangleq (x_1^T, x_2^T)^T$ for convenience. Let $x(\cdot)$ denote the vector function with $x(t) = [x_1(t), x_2(t), \dots, x_n(t)] \in R^n$ for all $t \in R$. $\|x(t)\|_\infty$ is the vector infinity-norm at time instant t such that $\|x(t)\|_\infty \triangleq \max_i |x_i(t)|$ and $\|x\|_\infty$ is function infinity-norm such that $\|x\|_\infty \triangleq \sup_{t \in R} \|x(t)\|_\infty$. Let \mathcal{L}_∞ denote the function space of bounded functions, i.e., $x \in \mathcal{L}_\infty$ implies that $\|x\|_\infty < \infty$, and $\|A\|_\infty$ denote the induced matrix infinity-norm of matrix $A \in R^{n \times m}$ such that $\|A\|_\infty \triangleq \max_i \sum_{j=1}^n |a_{ij}|$.

2.2 Input-output Feedback Linearization of MIMO System

We recall the method of input-output feedback linearization for square MIMO systems (Slotine and Li, 1991, Chapter 6) and (Isidori, 1995, Chapter 5) (see also Liu *et al.*). Consider the square system

$$\dot{x} = f(x) + g(x)u, \quad y = h(x), \quad (1)$$

where $x \in R^n$ is the state vector, $u \in R^m$ is the control input, $y \in R^m$ the system output, f , h and g are smooth vector fields. Assume that r_i is the smallest integer such that at least one of the inputs appears in $\frac{d^{r_i}y_i}{dt^{r_i}}$ for the output y_i . This yields

$$\begin{aligned} \begin{pmatrix} \frac{d^{r_1}y_1}{dt^{r_1}} \\ \vdots \\ \frac{d^{r_m}y_m}{dt^{r_m}} \end{pmatrix} &= \begin{pmatrix} \mathcal{L}_f^{r_1}h_1(x) \\ \vdots \\ \mathcal{L}_f^{r_m}h_m(x) \end{pmatrix} + \begin{pmatrix} \sum_{j=1}^m \mathcal{L}_{g_j}\mathcal{L}_f^{r_1-1}h_j(x)u_j \\ \vdots \\ \sum_{j=1}^m \mathcal{L}_{g_j}\mathcal{L}_f^{r_m-1}h_j(x)u_j \end{pmatrix} \\ &\triangleq \mathcal{L}_f^r h(x) + E(x)u, \end{aligned} \quad (2)$$

where $\mathcal{L}_{g_j}\mathcal{L}_f^{r_i-1}h_j(x) \neq 0$, $i = 1, \dots, m$ for at least one j , in a neighborhood χ_i of the point x_0 . Then, the system (1) is said to have a vector relative degree $r = (r_1, \dots, r_m)$ at x_0 . Define χ as the intersection of the χ_i and assume $E(x)$ is invertible over the region χ . Then, the input transformation

$$u = E^{-1}(x)(v - \mathcal{L}_f^r h(x)), \quad (3)$$

yields m equations of the simple form

$$\frac{d^{r_i}y_i}{dt^{r_i}} = v_i, \quad (4)$$

that is, the system is input-output linearized. Let the mapping z represents the output y and its time derivatives up to the vector relative degree $r - 1$,

$$z \triangleq \left(h_1(x), \mathcal{L}_f^1 h_1(x), \dots, \mathcal{L}_f^{r_1-1} h_1(x), \dots, h_m(x), \mathcal{L}_f^1 h_m(x), \dots, \mathcal{L}_f^{r_m-1} h_m(x) \right) \quad (5)$$

If $r_1 + \dots + r_m < n$, it is always possible to find $n - (r_1 + \dots + r_m)$ more functions $\eta \in R^{n-(r_1+\dots+r_m)}$ such that the mapping $(z, \eta) = \Phi(x)$ has a Jacobian matrix $\Delta\Phi(x_0)$ which is nonsingular at x_0 . The value at x_0 of these additional functions can be fixed arbitrarily. Then, (z, η) forms a locally valid change of coordinates. In the new coordinates (z, η) and with the input transformation (3), the system (1) can be described by (4) together with an equation of the form,

$$\dot{\eta} = s_1(\eta, z) + s_2(\eta, z)v. \quad (6)$$

To maintain exact output tracking $y = y_d$ (i.e., such that $z = z_d$) where the subscript d represents the desired value, we must have $v_i = \frac{d^{r_i}y_{i,d}}{dt^{r_i}}$ in which case the dynamics (6) are of the form,

$$\dot{\eta} = s(\eta, z_d, \dot{z}_d) \triangleq (\eta, Y_d) \quad (7)$$

for some functions $s(\cdot, \cdot)$ sufficiently smooth, where $Y_d \triangleq \left(y_{1,d}, \dots, \frac{d^{r_1}y_{1,d}}{dt}, \dots, y_{m,d}, \dots, \frac{d^{r_m}y_{m,d}}{dt} \right)$. The dynamics (7) are called the internal dynamics. They are driven by the reference output trajectory y_d .

2.3 Nonlinear Stable Inversion Problem

We review the nonlinear stable inversion technique proposed in Devasia *et al.* (1996) and also Zou and Devasia (2004). Consider the nonlinear, time-invariant, square system with m inputs and m outputs (1). Assume that the origin is an equilibrium point of the system when the inputs are zero. Given a sufficiently smooth, desired output trajectory $y_d(\cdot)$, the nonlinear stable-inversion problem is to find a bounded input and associated state trajectory $(u_{ff}(\cdot), x_d(\cdot))$, such that:

- (i) $\dot{x}_d(t) = f(x_d(t)) + g(x_d(t))u_{ff}(t)$ (see equations (1)) is satisfied for all time $t \in (-\infty, \infty)$;
- (ii) exact output tracking is achieved for all time $t \in (-\infty, \infty)$, $y_d(t) = h(x_d(t))$;
- (iii) the input and states are bounded in time, i.e., $x_d \in \mathcal{L}_\infty$ and $u_{ff} \in \mathcal{L}_\infty$.

Remark 1 The solution of the nonlinear stable-inversion problem results in inputs that are noncausal for non-minimum phase systems.

It will be shown that finding such a bounded input u_{ff} is equivalent to finding a bounded solution to the internal dynamics of the system (1). Then, a bounded solution to the internal dynamics will be found by using a Picard-like iteration process.

2.4 Iterative Solution to the Inversion Problem

The stable inversion procedure for finding the bounded solutions to the internal dynamics is reviewed as follows.

Step 1: the internal dynamics (7) is rewritten as

$$\begin{aligned} \dot{\eta}(t) &= A_\eta \eta(t) + (s(\eta(t), Y_d(t)) - A_\eta \eta(t)) \\ &\triangleq A_\eta \eta(t) + \psi(\eta(t), Y_d(t)), \end{aligned} \tag{8}$$

where $A_\eta = \left. \frac{\partial s(\eta(t), Y_d(t))}{\partial \eta} \right|_{Y_d=0, \eta=0}$.

Step 2: we suppose that the linearization of the internal dynamics (7) is hyperbolic, that is, A_η has the form

$$A_\eta = \begin{pmatrix} A_s & 0 \\ 0 & A_u \end{pmatrix} \tag{9}$$

such that the eigenvalues of A_s and A_u are on the left side and the right side of the imaginary axis in the complex plane respectively.

Step 3: Using a Picard-like iteration one finds the bounded solution to the nonlinear internal dynamics (7) for all $t \in R$ by solving the following iteration $i \geq 1$ of linear equations,

$$\begin{aligned} \dot{\eta}_{s,i}(t) &= A_s \eta_{s,i}(t) + I_s \psi(\eta_{s,i-1}(t), \eta_{u,i-1}(t), Y_d(t)) \\ &\triangleq A_s \eta_{s,i}(t) + \psi_{s,i-1}(t) \\ \dot{\eta}_{u,i}(t) &= A_u \eta_{u,i}(t) + I_u \psi(\eta_{s,i-1}(t), \eta_{u,i-1}(t), Y_d(t)) \\ &\triangleq A_u \eta_{u,i}(t) + \psi_{u,i-1}(t), \end{aligned} \tag{10}$$

where the identity matrix $I = [I_s, I_u] \in R^{n_\eta \times n_\eta}$, is partitioned according to the row dimensions of A_s and A_u . Let $\eta_{s,0} = \eta_{u,0} = 0$ the initial solution of the internal dynamics. For each iteration step $i \geq 1$, the linearized internal dynamics (10) is solved by flowing the stable internal dynamics $\eta_{s,i}$ forward in time and

the unstable internal dynamics $\eta_{u,i}$ backward in time,

$$\begin{aligned} \begin{pmatrix} \eta_{s,i}(t) \\ \eta_{u,i}(t) \end{pmatrix} &= \begin{pmatrix} \int_{-\infty}^t \Phi_s(t, \tau) \psi_{s,i-1}(\tau) d\tau \\ -\int_t^{\infty} \Phi_u(t, \tau) \psi_{u,i-1}(\tau) d\tau \end{pmatrix} \\ &\triangleq \mathcal{S}(\eta_{i-1}(\cdot), Y_d(\cdot))(t), \end{aligned} \quad (11)$$

where $\Phi_s(t, \tau) = e^{A_s(t-\tau)}$, $\Phi_u(t, \tau) = e^{-A_u(\tau-t)}$ are the state transition matrices.

2.5 Convergence of the Iterative Inversion Approach

Convergence of the iterative inversion procedure depends on the hyperbolicity (see Devasia (1999) for the case on the non-hyperbolicity) and the nonlinearity of the internal dynamics.

Assumption 1: Suppose that the right hand side of internal dynamics (7) are sufficiently smooth. (8) and (9) are satisfied.

Assumption 2: By hyperbolicity, there exist positive constants $K, \alpha, \beta > 0$ such that for any $t_1 \geq t_2$,

$$\|\Phi_s(t_1, t_2)\|_{\infty} \leq K e^{-\alpha(t_1-t_2)}, \quad \|\Phi_u(t_2, t_1)\|_{\infty} \leq K e^{-\beta(t_1-t_2)}. \quad (12)$$

Assumption 3: Assume that the nonlinear perturbation terms $\psi(\cdot, \cdot)$ in (8) is locally Lipschitz about the origin. There exist positive constants K_1, K_2, r_Y and r_{η} such that for any $\|Y(\cdot)\|_{\infty}, \|\hat{Y}(\cdot)\|_{\infty} \leq r_Y$ and $\|\eta(\cdot)\|_{\infty}, \|\hat{\eta}(\cdot)\|_{\infty} \leq r_{\eta}$,

$$\|\psi(\eta(t), Y(t)) - \psi(\hat{\eta}(t), \hat{Y}(t))\|_{\infty} \leq K_1 \|\eta(t) - \hat{\eta}(t)\|_{\infty} + K_2 \|Y(t) - \hat{Y}(t)\|_{\infty}, \quad (13)$$

uniformly in $t \in R$.

Condition 1: Given K_1, K_2 as defined in (13) and K, α, β as defined in (12), the following inequalities are satisfied,

$$K_1 K \max(1/\alpha, 1/\beta) \triangleq K_{\alpha\beta,1} < 1, \quad K_2 K \max(1/\alpha, 1/\beta) \triangleq K_{\alpha\beta,2} < 1 - K_{\alpha\beta,1}. \quad (14)$$

The main result of the stable-inversion theory which is proposed in Devasia *et al.* (1996) and Zou and Devasia (2004) is.

THEOREM 2.1 (Devasia *et al.* (1996); Zou and Devasia (2004)) *Let Assumptions 1, 2, 3 and Condition 1 be satisfied; then,*

1) *there exists a locally unique fixed point $\eta^*(\cdot) \in \mathcal{L}_{\infty}$ of the mapping $\eta^*(t) = (\eta_s^*(t), \eta_u^*(t)) = \mathcal{S}(\eta^*(\cdot), Y_d(\cdot))(t), \forall t \in R$;*

2) *the fixed point $\eta^*(\cdot)$ is a bounded solution to the internal dynamics (7) and can be found by the Picard-like iteration process (11);*

3) *Exact output tracking is achieved for $t \in (-\infty, \infty)$ by using the following inverse input $u_{ff}^*(t) \triangleq q(\eta^*(t), Y_d(t))$.*

3 Exact Output Tracking Problem of the Spherical Inverted Pendulum

3.1 Modeling

Let the globally fixed inertial coordinate frame be $\{C\}$ in Cartesian coordinates (x, y, z) with the origin attached to the bottom of the pendulum. Let the body-fixed frame be $\{B\}$ in Cartesian coordinates (X, Y, Z) with the origin attached to the center of mass of the pendulum. Let the 4-dimensional configuration space $Q = S \times G$ where S denotes shape space, G denotes Abelian group. We consider a spherical inverted

pendulum in the generalized coordinates $q \triangleq (x, y, X, Y) \in Q$ suggested in Bloch *et al.* (2001) (see Fig. 1). $(x, y) \in G$ denote translational coordinates of the pendulum in the local chart $\{C\}$ and there are two independent controls (F_x, F_y) that can move the pendulum in x and y directions. $(X, Y) \in S$ denote the shape positions of the beam in the local chart $\{B\}$ where (X, Y) is the projections of the center of mass on the horizontal plane. Here, we assume that the pendulum is a slim cylindrical beam with the uniform mass density other than the simplified spherical inverted pendulum on the cart where the pendulum is the bob with mass m supported by a massless pole in Bloch *et al.* (2001). Modeling for the same object (see Figure 1) was also given in Liu *et al.* (2005); Liu *et al.* by using other two sets of coordinates.

The space above the horizontal plane is called the ‘‘upper half space’’. The ‘‘upper half space’’ is defined as $U \triangleq \{\sqrt{X^2 + Y^2} < L\}$. U represents the ‘‘upper half space’’ in the sequel.

As shown in Figure 2, an infinitesimal section with the length dl along the beam with the cross section area \mathcal{A} is regarded as a particle with volume $\mathcal{A} \cdot dl$, the mass of the infinitesimal section (resp. the particle) is $\frac{m}{2L\mathcal{A}}\mathcal{A}dl = \frac{m}{2L}dl$ where l is the length of the particle to the pivot and the velocity vector of the particle is $V_l = \left(\dot{x} + \frac{l\dot{X}}{L}, \dot{y} + \frac{l\dot{Y}}{L}, \frac{l}{L} \frac{X\dot{X} + Y\dot{Y}}{\sqrt{L^2 - X^2 - Y^2}} \right)$.

The kinetic energy of the pendulum can be expressed as the sum of the kinetic energy of all particles along the beam

$$\begin{aligned}
 T &= \frac{1}{2} \int_0^{2L} \frac{m}{2L} \langle V_l, V_l \rangle dl, \\
 &= \frac{1}{2} \begin{pmatrix} \dot{x} \\ \dot{y} \\ \dot{X} \\ \dot{Y} \end{pmatrix}^T \begin{pmatrix} m & 0 & m & 0 \\ 0 & m & 0 & m \\ m & 0 & \frac{4m}{3} \frac{L^2 - Y^2}{L^2 - X^2 - Y^2} & \frac{4m}{3} \frac{XY}{L^2 - X^2 - Y^2} \\ 0 & m & \frac{4m}{3} \frac{XY}{L^2 - X^2 - Y^2} & \frac{4m}{3} \frac{L^2 - X^2}{L^2 - X^2 - Y^2} \end{pmatrix} \begin{pmatrix} \dot{x} \\ \dot{y} \\ \dot{X} \\ \dot{Y} \end{pmatrix}. \tag{15}
 \end{aligned}$$

The total potential energy is given by

$$V \triangleq mg(\sqrt{L^2 - X^2 - Y^2} - L). \tag{16}$$

We define the Lagrangian of the pendulum $\mathcal{L} : TQ \mapsto Q$

$$\mathcal{L} = T(\dot{x}, \dot{y}, X, Y, \dot{X}, \dot{Y}) - V(X, Y), \tag{17}$$

which is independent of (x, y) , the cyclic variables.

The equations of motion are given by

$$\frac{d}{dt} \frac{\partial \mathcal{L}}{\partial \dot{q}_i} - \frac{\partial \mathcal{L}}{\partial q_i} = Q_i \quad \text{for } i = 1, 2, 3, 4. \tag{18}$$

These can be expressed as (see Appendix A for details)

$$\ddot{q}_i = D^{-1}(q) \cdot (Q_i - C(q, \dot{q})\dot{q}_i - G(q)). \tag{19}$$

where

$$D(q) = \begin{pmatrix} m & 0 & m & 0 \\ 0 & m & 0 & m \\ m & 0 & \frac{4m}{3} \frac{L^2 - Y^2}{L^2 - X^2 - Y^2} & \frac{4m}{3} \frac{XY}{L^2 - X^2 - Y^2} \\ 0 & m & \frac{4m}{3} \frac{XY}{L^2 - X^2 - Y^2} & \frac{4m}{3} \frac{L^2 - X^2}{L^2 - X^2 - Y^2} \end{pmatrix}, \quad G(q) = \begin{pmatrix} 0 \\ 0 \\ \frac{-mgX}{\sqrt{L^2 - X^2 - Y^2}} \\ \frac{-mgY}{\sqrt{L^2 - X^2 - Y^2}} \end{pmatrix}, \quad Q_i = \begin{pmatrix} F_x + v_{f_1} \\ F_y + v_{f_2} \\ v_{f_3} \\ v_{f_4} \end{pmatrix},$$

$$C(q, \dot{q}) = \begin{pmatrix} 0 & 0 & 0 & 0 \\ 0 & 0 & 0 & 0 \\ 0 & 0 & \frac{4mX(\dot{X}(L^2 - Y^2) + 2XY\dot{Y})}{3(L^2 - X^2 - Y^2)^2} & \frac{4mX\dot{Y}(L^2 - X^2)}{3(L^2 - X^2 - Y^2)^2} \\ 0 & 0 & \frac{4mY\dot{X}(L^2 - Y^2)}{3(L^2 - X^2 - Y^2)^2} & \frac{4mY(\dot{Y}(L^2 - X^2) + 2XY\dot{X})}{3(L^2 - X^2 - Y^2)^2} \end{pmatrix}.$$

Table 1. Nomenclature for the spherical inverted pendulum

Name	Symbol	Unit	Simulation Value
Generalized Coordinates	(x, y, X, Y)	m	-
Shape Variables	(X, Y)	m	-
External Variables	(x, y)	m	-
The Length	$2 \times L$	m	0.6
The Mass	m	kg	0.35
Gravity	g	m/s^2	9.8
Actuation Forces	F_x, F_y	N	-
Disturbance	v_f	N	-
Viscous Friction Coefficients	C_x, C_y, C_X, C_Y	$N \cdot s/m$	1×10^{-3}

3.2 Problem Formulation

The problem of exact output tracking for the spherical inverted pendulum can be formulated as follows.

[Exact Output tracking]: Consider the equations of dynamics (19) for the spherical inverted pendulum. Let $(x_d(t), y_d(t))$ for $t \in (-\infty, \infty)$ be a sufficiently smooth desired curvature in the globally fixed frame $\{C\}$. Derive a feedback control law for $F \triangleq (F_x, F_y)$ such that the pivot position (x, y) of the pendulum converges to $(x_d(t), y_d(t))$ asymptotically, i.e., $x(t) - x_d(t) \rightarrow 0$, $y(t) - y_d(t) \rightarrow 0$ as $t \rightarrow \infty$. Meanwhile, the pendulum is kept in U .

4 Control Design

4.1 The Strategy

In the design, we consider the generalized control force¹ to be

$$\{Q\} = (F_x, F_y, 0, 0) \text{ or } v_f \equiv 0. \quad (20)$$

We proceed with the design in three stages as outlined in Section 1.

¹In the simulation study, v_f is not zero (so as to test robustness).

4.2 Partially Feedback Linearization

We rewrite the dynamics as follows

$$\begin{aligned} \begin{pmatrix} \ddot{x} \\ \ddot{y} \\ \ddot{X} \\ \ddot{Y} \end{pmatrix} &= \begin{pmatrix} \alpha_{11}(X, Y) & \alpha_{12}(X, Y) \\ \alpha_{21}(X, Y) & \alpha_{22}(X, Y) \\ \alpha_{31}(X, Y) & \alpha_{32}(X, Y) \\ \alpha_{41}(X, Y) & \alpha_{42}(X, Y) \end{pmatrix} F + \begin{pmatrix} \beta_1(X, \dot{X}, Y, \dot{Y}) \\ \beta_2(X, \dot{X}, Y, \dot{Y}) \\ \beta_3(X, \dot{X}, Y, \dot{Y}) \\ \beta_4(X, \dot{X}, Y, \dot{Y}) \end{pmatrix} \\ &\triangleq \begin{pmatrix} H_{11}(X, Y) \\ H_{21}(X, Y) \end{pmatrix} F + \begin{pmatrix} H_{12}(X, \dot{X}, Y, \dot{Y}) \\ H_{22}(X, \dot{X}, Y, \dot{Y}) \end{pmatrix} \end{aligned} \tag{21}$$

where $H_{11}(X, Y)$, $H_{21}(X, Y)$, $H_{12}(X, \dot{X}, Y, \dot{Y})$, $H_{22}(X, \dot{X}, Y, \dot{Y})$ are explicitly given in Appendix B. Also notice that $H_{11}(X, Y)$ is invertible on U .

Complete now a partial input-output feedback linearization. Let the output vector be (x, y, X, Y) . We have

$$\begin{pmatrix} \ddot{x} \\ \ddot{y} \\ \ddot{X} \\ \ddot{Y} \end{pmatrix} = \begin{pmatrix} H_{11}(X, Y) \\ H_{21}(X, Y) \end{pmatrix} F + \begin{pmatrix} H_{12}(X, \dot{X}, Y, \dot{Y}) \\ H_{22}(X, \dot{X}, Y, \dot{Y}) \end{pmatrix}, \tag{22}$$

which implies that system (21) has vector relative degree $r = (2, 2, 2, 2)$. $\begin{pmatrix} H_{11}(X, Y) \\ H_{21}(X, Y) \end{pmatrix}$ is not square because of the underactuated system (21), i.e., $F \in R^2$, $q \in R^4$. We achieve partial feedback linearization with for example

$$F = H_{11}^{-1}(X, Y)(v - H_{12}(X, \dot{X}, Y, \dot{Y})), \tag{23}$$

where $v = (v_1, v_2)$ is a new input vector. This leads us to

$$\begin{pmatrix} \ddot{x} \\ \ddot{y} \\ \ddot{X} \\ \ddot{Y} \end{pmatrix} = \begin{pmatrix} v \\ H_{21}(X, Y) \left(H_{11}^{-1}(X, Y) \cdot (v - H_{12}(X, \dot{X}, Y, \dot{Y})) \right) + H_{22}(X, \dot{X}, Y, \dot{Y}) \end{pmatrix}, \tag{24}$$

where (\ddot{X}, \ddot{Y}) equations lead to the internal dynamics.

Now, consider the system (24) instead of (21), assign a control function to v and come back to the original system (21) at the end of the design. Let $z \triangleq (x, \dot{x}, y, \dot{y}, X, \dot{X}, Y, \dot{Y})$ be the state vector. we rewrite the system (24) in state space

$$\begin{pmatrix} \dot{z}_1 \\ \dot{z}_2 \\ \dot{z}_3 \\ \dot{z}_4 \\ \dot{z}_5 \\ \dot{z}_6 \\ \dot{z}_7 \\ \dot{z}_8 \end{pmatrix} = \begin{pmatrix} z_2 \\ v_1 \\ z_4 \\ v_2 \\ z_6 \\ f_6(z_5, z_6, z_7, z_8, v_1, v_2) \\ z_8 \\ f_8(z_5, z_6, z_7, z_8, v_1, v_2) \end{pmatrix}, \tag{25}$$

where functions f_6 and f_8 are given as follows

$$\begin{pmatrix} f_6(\cdot) \\ f_8(\cdot) \end{pmatrix} = \begin{pmatrix} \frac{3(L^2 - z_5^2)}{4L^2} (z_5 \cdot f_{term} - v_1) - \frac{3z_5 z_7}{4L^2} (z_7 \cdot f_{term} - v_2) \\ \frac{3(L^2 - z_7^2)}{4L^2} (z_7 \cdot f_{term} - v_2) - \frac{3z_5 z_7}{4L^2} (z_5 \cdot f_{term} - v_1) \end{pmatrix}$$

with $f_{term} = -\frac{4(L^2(z_6^2 + z_8^2) - (z_6 z_7 - z_8 z_5)^2)}{3(L^2 - z_5^2 - z_7^2)^2} + \frac{g}{\sqrt{L^2 - z_5^2 - z_7^2}}$.

Let $Y_d(t) = (x_d(t), \dot{x}_d(t), \ddot{x}_d(t), y_d(t), \dot{y}_d(t), \ddot{y}_d(t))$ represents the desired output trajectories and their time derivatives up to the vector relative degree $r = (2, 2)$. Obviously, we have $(z_{1_d}(t), z_{2_d}(t), z_{3_d}(t), z_{4_d}(t)) = (x_d(t), \dot{x}_d(t), y_d(t), \dot{y}_d(t)) \in Y_d(t)$ and $v_d(t) = (\ddot{x}_d(t), \ddot{y}_d(t)) \in Y_d(t)$ be some desired states and the desired feedforward inputs (i.e., the guidance control) respectively.

Let $\zeta \triangleq (z_5, z_6, z_7, z_8)$ and $s(\zeta, v_d) \triangleq (z_6, f_{z_6}, z_8, f_{z_8})$. Then, the internal dynamics with respect to the general case (7) is of the form

$$\dot{\zeta} = s(\zeta, v_d). \tag{26}$$

4.3 Stable Inversion and Achievable Trajectories

Our task is to find the bounded trajectories of the internal dynamics with respect to the bounded input $v_{ff}(t) = (\ddot{x}_d(t), \ddot{y}_d(t))$. The bounded solutions to the internal dynamics can be found through stable inversion and then we obtain the pair of desired inputs and states (v_{ff}, z_d) .

We rewrite the internal dynamics (26) in a perturbed linear system

$$\dot{\zeta} = A_\zeta \zeta + [s(\zeta, v_{ff}) - A_\zeta \zeta]. \tag{27}$$

where $A_\zeta = \left. \frac{\partial s(\zeta, v_{ff})}{\partial \zeta} \right|_{\zeta=0, v=0} = \begin{pmatrix} 0 & 1 & 0 & 0 \\ \frac{3g}{4L} & 0 & 0 & 0 \\ 0 & 0 & 0 & 1 \\ 0 & 0 & \frac{3g}{4L} & 0 \end{pmatrix}$.

The matrix A_ζ have two pairs of repeated eigenvalues $\pm \sqrt{\frac{3g}{4L}}$. Since A_ζ is in the desired form (9), we use a state space transformation:

$$P \triangleq \begin{pmatrix} 1 & 0 & 1 & 0 \\ -\sqrt{\frac{3g}{4L}} & 0 & \sqrt{\frac{3g}{4L}} & 0 \\ 0 & 1 & 0 & 1 \\ 0 & -\sqrt{\frac{3g}{4L}} & 0 & \sqrt{\frac{3g}{4L}} \end{pmatrix} \text{ and } P^{-1} = \begin{pmatrix} \frac{1}{2} & -\frac{1}{2}\sqrt{\frac{4L}{3g}} & 0 & 0 \\ 0 & 0 & \frac{1}{2} & -\frac{1}{2}\sqrt{\frac{4L}{3g}} \\ \frac{1}{2} & \frac{1}{2}\sqrt{\frac{4L}{3g}} & 0 & 0 \\ 0 & 0 & \frac{1}{2} & \frac{1}{2}\sqrt{\frac{4L}{3g}} \end{pmatrix} \tag{28}$$

to obtain a new transition matrix

$$\begin{aligned} A_\eta &\triangleq P^{-1} A_\zeta P \\ &= \text{diag} \left(-\sqrt{\frac{3g}{4L}}, -\sqrt{\frac{3g}{4L}}, \sqrt{\frac{3g}{4L}}, \sqrt{\frac{3g}{4L}} \right) \\ &\triangleq \text{diag}(A_s, A_u). \end{aligned} \tag{29}$$

We take a change of coordinates $\zeta \triangleq P\eta$ and the internal dynamics (27) in new states η

$$\begin{aligned} \dot{\eta} &= A_\eta \eta + P^{-1}[s(P\eta, v_{ff}) - A_\zeta P\eta] \\ &= A_\eta \eta + [P^{-1}s(P\eta, v_{ff}) - A_\eta \eta] \\ &\triangleq A_\eta \eta + \psi(\eta(t), v_{ff}) \end{aligned} \tag{30}$$

where the entries $\psi(\eta, v_{ff})$ are given by

$$\psi(\eta, v_{ff}) = \begin{pmatrix} -\sqrt{\frac{L}{3g}} \left(\frac{3(L^2 - (\eta_1 + \eta_2)^2)}{4L^2} ((\eta_1 + \eta_2) \cdot f_{term} - \ddot{x}_d) - \frac{3(\eta_1 + \eta_2)(\eta_3 + \eta_4)}{4L^2} ((\eta_3 + \eta_4) \cdot f_{term} - \ddot{y}_d) \right) + \frac{1}{4} \sqrt{\frac{3g}{L}} (\eta_1 + \eta_2) \\ -\sqrt{\frac{L}{3g}} \left(\frac{3(L^2 - (\eta_3 + \eta_4)^2)}{4L^2} ((\eta_3 + \eta_4) \cdot f_{term} - \ddot{y}_d) - \frac{3(\eta_1 + \eta_2)(\eta_3 + \eta_4)}{4L^2} ((\eta_1 + \eta_2) \cdot f_{term} - \ddot{x}_d) \right) + \frac{1}{4} \sqrt{\frac{3g}{L}} (\eta_3 + \eta_4) \\ \sqrt{\frac{L}{3g}} \left(\frac{3(L^2 - (\eta_1 + \eta_2)^2)}{4L^2} ((\eta_1 + \eta_2) \cdot f_{term} - \ddot{x}_d) - \frac{3(\eta_1 + \eta_2)(\eta_3 + \eta_4)}{4L^2} ((\eta_3 + \eta_4) \cdot f_{term} - \ddot{y}_d) \right) - \frac{1}{4} \sqrt{\frac{3g}{L}} (\eta_1 + \eta_2) \\ \sqrt{\frac{L}{3g}} \left(\frac{3(L^2 - (\eta_3 + \eta_4)^2)}{4L^2} ((\eta_3 + \eta_4) \cdot f_{term} - \ddot{y}_d) - \frac{3(\eta_1 + \eta_2)(\eta_3 + \eta_4)}{4L^2} ((\eta_1 + \eta_2) \cdot f_{term} - \ddot{x}_d) \right) - \frac{1}{4} \sqrt{\frac{3g}{L}} (\eta_3 + \eta_4) \end{pmatrix}$$

where

$$\begin{aligned} f_{term} &= -\frac{4L^2(((-\eta_1 + \eta_2)\sqrt{3g/(4L)})^2 + ((-\eta_3 + \eta_4)\sqrt{3g/(4L)})^2)}{3(L^2 - (\eta_1 + \eta_2)^2 - (\eta_3 + \eta_4)^2)^2} \\ &\quad + \frac{4(((-\eta_1 + \eta_2)\sqrt{3g/(4L)})(\eta_3 + \eta_4) - ((-\eta_3 + \eta_4)\sqrt{3g/(4L)})(\eta_1 + \eta_2))^2}{3(L^2 - (\eta_1 + \eta_2)^2 - (\eta_3 + \eta_4)^2)^2} \\ &\quad + \frac{g}{\sqrt{L^2 - (\eta_1 + \eta_2)^2 - (\eta_3 + \eta_4)^2}}. \end{aligned}$$

To apply Theorem (2.1) successfully, we must check whether the Assumptions 1, 2, 3 and Condition 1 are satisfied.

To satisfy Assumption 1, we restrict the desired output profile $(x_d(t), y_d(t))$ to be C^2 functions.

Let $\alpha \triangleq \sqrt{\frac{3g}{4L}}$, $\beta \triangleq \sqrt{\frac{3g}{4L}}$ and $K = 1$ such that Assumption 2 is satisfied.

The nonlinear perturbation terms $\psi(\cdot, \cdot)$ are analytic because $\psi(\cdot, \cdot)$ are functions of analytical functions and are locally Lipschitz about the origin because $L^2 - z_{5_d}^2 - z_{7_d}^2 \geq \varepsilon^*$ for some $\varepsilon^* > 0$ is assumed so as that the positive denominators in $\psi(\cdot, \cdot)$ are assumed. Then, there exists positive constants K_1, K_2, r_v and r_η such that for any $\|v_{ff}(\cdot)\|_\infty, \|\hat{v}_{ff}(\cdot)\|_\infty \leq r_v$ and $\|\eta(\cdot)\|_\infty, \|\hat{\eta}(\cdot)\|_\infty \leq r_\eta$

$$\|\psi(\eta(t), v_{ff}(t)) - \psi(\hat{\eta}(t), \hat{v}_{ff}(t))\|_\infty \leq K_1 \|\eta - \hat{\eta}\|_\infty + K_2 \|v_{ff}(t) - \hat{v}_{ff}(t)\|_\infty, \tag{31}$$

for all $t \in R$. Hence, Assumption 3 is satisfied.

By Condition 1, we let $K_{\alpha\beta,1} \triangleq \sqrt{\frac{4L}{3g}} K_1 < 1$ and $K_{\alpha\beta,2} \triangleq \sqrt{\frac{4L}{3g}} K_2 < 1 - K_{\alpha\beta,1}$. Thus, the positive constants K_1 and K_2 must satisfy

$$K_1 + K_2 < \sqrt{\frac{3g}{4L}}. \tag{32}$$

In reverse, K_1 and K_2 satisfying (32) determine the constants r_v and r_η in (31). Based upon constants r_v and r_η defined as the above, Condition 1 can be satisfied.

Theorem 2.1 may be applied and there exists a unique fixed point $\eta^*(t)$, i.e., the desired trajectories $\eta_d(t)$ which is the bounded solution of the internal dynamics. $\eta^*(t)$ is found through the Picard-like iteration

for all $t \in R$ by solving the following iterations $i \geq 1$ of linear equations (see (10)),

$$\begin{aligned} \begin{pmatrix} \dot{\eta}_{1,i} \\ \dot{\eta}_{2,i} \end{pmatrix} &= A_s \begin{pmatrix} \eta_{1,i}(t) \\ \eta_{2,i}(t) \end{pmatrix} + \begin{pmatrix} \psi_{1,i-1}(\eta_{1,i-1}(t), \eta_{2,i-1}(t), \eta_{3,i-1}(t), \eta_{4,i-1}(t), \ddot{x}_d, \ddot{y}_d) \\ \psi_{2,i-1}(\eta_{1,i-1}(t), \eta_{2,i-1}(t), \eta_{3,i-1}(t), \eta_{4,i-1}(t), \ddot{x}_d, \ddot{y}_d) \end{pmatrix} \\ \begin{pmatrix} \dot{\eta}_{3,i} \\ \dot{\eta}_{4,i} \end{pmatrix} &= A_u \begin{pmatrix} \eta_{3,i}(t) \\ \eta_{4,i}(t) \end{pmatrix} + \begin{pmatrix} \psi_{3,i-1}(\eta_{1,i-1}(t), \eta_{2,i-1}(t), \eta_{3,i-1}(t), \eta_{4,i-1}(t), \ddot{x}_d, \ddot{y}_d) \\ \psi_{4,i-1}(\eta_{1,i-1}(t), \eta_{2,i-1}(t), \eta_{3,i-1}(t), \eta_{4,i-1}(t), \ddot{x}_d, \ddot{y}_d) \end{pmatrix}. \end{aligned} \quad (33)$$

For each iteration step $i \geq 1$, the internal dynamics (33) is solved by flowing the stable internal dynamics $(\eta_{1,i}, \eta_{2,i})$ forward in time and the unstable internal dynamics $(\eta_{3,i}, \eta_{4,i})$ backward in time,

$$\begin{aligned} \begin{pmatrix} \eta_{1,i}(t) \\ \eta_{2,i}(t) \\ \eta_{3,i}(t) \\ \eta_{4,i}(t) \end{pmatrix} &= \begin{pmatrix} \int_{-\infty}^t \Phi_s(t, \tau) \psi_{1,i-1}(\tau) d\tau \\ \int_{-\infty}^t \Phi_s(t, \tau) \psi_{2,i-1}(\tau) d\tau \\ - \int_t^{\infty} \Phi_u(t, \tau) \psi_{3,i-1}(\tau) d\tau \\ - \int_t^{\infty} \Phi_u(t, \tau) \psi_{4,i-1}(\tau) d\tau \end{pmatrix} \\ &\triangleq \mathcal{S}(\eta_{i-1}(\cdot), Y_d(\cdot))(t), \end{aligned} \quad (34)$$

where $\Phi_s(t, \tau) = e^{A_s(t-\tau)} = e^{-\sqrt{\frac{3g}{4L}}(t-\tau)}$, $\Phi_u(t, \tau) = e^{-A_u(\tau-t)} = e^{-\sqrt{\frac{3g}{4L}}(t-\tau)}$.

By the relationship $\zeta_d(t) = P\eta_d(t)$, we obtain the desired trajectories of internal dynamics $\zeta_d(t) = (z_{5_d}(t), z_{6_d}(t), z_{7_d}(t), z_{8_d}(t))$. Furthermore, the output profiles and their time derivatives $(z_{1_d}(t), z_{2_d}(t), z_{3_d}(t), z_{4_d}(t)) = (x_d, \dot{x}_d, y_d, \dot{y}_d)$ have been given from the context. We obtain the desired state $z_d(t)$. So, we find the pair (v_{ff}, z_d) .

[Achievable trajectories]: the achievable trajectories for the spherical inverted pendulum in the context of stable inversion technique are defined to be those output profiles (x_d, y_d) which are $C^2(-\infty, \infty)$ functions and the desired inputs $v_{ff} \triangleq (\ddot{x}_d, \ddot{y}_d)$ are bounded such that for $\alpha = \beta = \sqrt{\frac{3g}{4L}}$, $K = 1$, and K_1, K_2 satisfying (32) and (31), and the bounded solution $\eta_d(t)$ of internal dynamics can be found through stable inversion technique. Thus, the pair (v_{ff}, z_d) can be found.

Remark 1 It may be observed that this is not the entire class of achievable output functions. Indeed, any motion along a straight line at constant speed is also an achievable trajectory. We have limited the space of desirable trajectories to lie in a compact set, which is not too restrictive form an application point of view.

In implementing a specific controller, we can choose some specific desired output trajectories in the family of achievable trajectories. We consider the desired output profiles $(x_d(t), y_d(t))$ where the unit t is the second for the translational positions:

$$x_d = \begin{cases} 0, & t < 0 \\ a(1 - \cos(\omega_1 t)), & 0 \leq t \leq 16\pi \\ 0, & t > 16\pi \end{cases}, \quad y_d = \begin{cases} 0, & t < 0 \\ b \sin(\omega_2 t), & 0 \leq t \leq 16\pi \\ 0, & t > 16\pi \end{cases} \quad (35)$$

The profile for output $(x_d(t), y_d(t))$ in (35) is non-smooth at $t = 0(s)$ and $t = 16\pi(s)$. Here, we slightly relax the condition that the output profiles $(x_d(t), y_d(t))$ are not C^2 everywhere but piecewise C^2 functions. Assumption 2, 3 and Condition 1 still hold. Therefore, these imperfections lead to some transient tracking errors at $t = 0$ and $t = 16\pi(s)$ but the internal state $\eta_d(t)$ is kept bounded. Taking the first and second time derivative of (x_d, y_d) gives

$$\dot{x}_d = \begin{cases} 0, & t < 0 \\ a\omega_1 \sin(\omega_1 t), & 0 \leq t \leq 16\pi \\ 0, & t > 16\pi \end{cases}, \quad \dot{y}_d = \begin{cases} 0, & t < 0 \\ b\omega_2 \cos(\omega_2 t), & 0 \leq t \leq 16\pi \\ 0, & t > 16\pi \end{cases} \quad (36)$$

$$\ddot{x}_d = \begin{cases} 0, & t < 0 \\ a\omega_1^2 \cos(\omega_1 t), & 0 \leq t \leq 16\pi \\ 0, & t > 16\pi \end{cases}, \quad \ddot{y}_d = \begin{cases} 0, & t < 0 \\ -b\omega_2^2 \sin(\omega_2 t), & 0 \leq t \leq 16\pi \\ 0, & t > 16\pi \end{cases} \quad (37)$$

Let $\omega_1 = \omega_2 = 0.5$ (hz), $a = 2$ (m), $b = 4$ (m). In this case, the path of the desired outputs is an ellipse in $t \in (0, 16\pi)(s)$ and a set-point in $t \in [16\pi, \infty)(s)$.

We can estimate whether or not the specific trajectories are achievable. We let $r_v = 1.12(N)$ such that $\|v_{ff}(\cdot)\|_\infty, \|\hat{v}_{ff}(\cdot)\|_\infty \leq r_v$. Let $L = 0.3$ (m), $g = 9.8$ (m/s²). Then, we have $K_1 + K_2 \leq 4.95$. Let $K_1 = K_2 = 2.45$ such that Condition 1 is satisfied. Noting that $\eta(\cdot)$ are unknown, we can not determine r_η satisfying (31) in advance. We can simplify the analysis here by assuming that there exists the positive number $r_\eta \ll L$, $\|\eta(\cdot)\|_\infty, \|\hat{\eta}(\cdot)\|_\infty \leq r_\eta$. In this case, we consider $L^2/(L^2 - (\eta_1 + \eta_2)^2 - (\eta_3 + \eta_4)^2) \approx 1$ and so on for the perturbation term $\psi(\eta(t), v_{ff}(t))$. Then, we can estimate the impact of the input v_{ff} to condition (31). If $r_\eta \ll L$, we have

$$\begin{aligned} & \|\psi(\eta(t), v_{ff}(t)) - \psi(\hat{\eta}(t), \hat{v}_{ff}(t))\|_\infty \approx \\ & \|\psi(\eta(t), 0) - \psi(\hat{\eta}(t), 0)\|_\infty + 0.08\|v_{ff}(t) - \hat{v}_{ff}(t)\|_\infty \end{aligned} \quad (38)$$

Suppose that

$$\|\psi(\eta(t), 0) - \psi(\hat{\eta}(t), \hat{0})\|_\infty \leq 2.45\|\eta - \hat{\eta}\|_\infty$$

hold. Noting that

$$0.08\|v_{ff}(t) - \hat{v}_{ff}(t)\|_\infty < 2.45\|v_{ff}(t) - \hat{v}_{ff}(t)\|_\infty$$

also hold, Assumption 3 is satisfied. Furthermore, Assumption 1, 2 are satisfied in general. A bounded solution $\eta(t)$ can be found through stable inversion. The above analysis implies that if the desired shape variables and their derivatives $(X_d, Y_d, \dot{X}_d, \dot{Y}_d)$ are sufficiently small and the initial conditions on (X, Y, \dot{X}, \dot{Y}) are close enough to $(X_d, Y_d, \dot{X}_d, \dot{Y}_d)$, the trajectory (35) are achievable by stable inversion. This assertion is verified by the simulation results in the next section.

4.4 Synthesizing the Feedforward and Feedback Control

In our case, the exact nonlinear output tracking control via the stable inversion tool is to find a control law

$$v = v_{ff} + v_{fb}, \quad (39)$$

where the feedforward control $v_{ff} = (\ddot{x}_d, \ddot{y}_d)$ is found through stable inversion and the feedback control is in a form $v_{fb} = \kappa(z_d(t) - z(t))$ where the desired states $z_d(t)$ are also found through inversion and the linear gain matrix κ is to be designed.

Step 1: we find the pair of bounded input and states $(v_{ff}(t), z_d(t))$. In the context, $v_{ff}(t) = (\ddot{x}_d, \ddot{y}_d)$ is the feedforward control.

Step 2: we assign a matrix κ such that the linearization of the system (25)

$$\dot{z} = Az + Bv, \quad (40)$$

where $A = \begin{pmatrix} 0 & 1 & 0 & 0 & 0 & 0 & 0 & 0 \\ 0 & 0 & 0 & 0 & 0 & 0 & 0 & 0 \\ 0 & 0 & 0 & 1 & 0 & 0 & 0 & 0 \\ 0 & 0 & 0 & 0 & 0 & 0 & 0 & 0 \\ 0 & 0 & 0 & 0 & 0 & 1 & 0 & 0 \\ 0 & 0 & 0 & 0 & \frac{3g}{4L} & 0 & 0 & 0 \\ 0 & 0 & 0 & 0 & 0 & 0 & 0 & 1 \\ 0 & 0 & 0 & 0 & 0 & 0 & \frac{3g}{4L} & 0 \end{pmatrix}$, $B = \begin{pmatrix} 0 & 0 \\ 1 & 0 \\ 0 & 0 \\ 0 & 1 \\ 0 & 0 \\ -\frac{3}{4} & 0 \\ 0 & 0 \\ 0 & -\frac{3}{4} \end{pmatrix}$ is stabilized by the feedback $v = -\kappa z$, that is,

$A - B\kappa$ is Hurwitz. Let some positive definite matrices $Q \in R^{8 \times 8}$ and $R \in R^{2 \times 2}$. Then, we use the linear optimal design tool—LQR to find an optimal matrix κ such that $A - B\kappa$ is Hurwitz. Finally, we assign $v_{fb} \triangleq \kappa(z_d(t) - z(t))$ the feedback part of the tracking control. For example, for $Q = \text{diag}(100, 20, 100, 20, 100, 20, 100, 20)$ and $R = \text{diag}(1, 1)$, we obtain an optimal gain matrix

$$\kappa = \begin{pmatrix} 10 & 10.4 & 0 & 0 & 177.5 & 36.11 & 0 & 0 \\ 0 & 0 & 10 & 10.4 & 0 & 0 & 177.5 & 36.11 \end{pmatrix}. \tag{41}$$

We wrap up all steps of the design and obtain the final control law in a form

$$\begin{pmatrix} F_x \\ F_y \end{pmatrix} = H_{11}^{-1}(X, Y) \cdot \left(\begin{pmatrix} \ddot{x}_d \\ \ddot{y}_d \end{pmatrix} + \kappa(z_d(t) - z(t)) - H_{12}(X, \dot{X}, Y, \dot{Y}) \right), \tag{42}$$

where $z_d(t) = (x_d, \dot{x}_d, y_d, \dot{y}_d, X_d, \dot{X}_d, Y_d, \dot{Y}_d)$ is found through the stable inversion technique.

Noting that without using stable inversion technique, we have only a feedback tracking control law in a form

$$\begin{pmatrix} F_x \\ F_y \end{pmatrix} = H_{11}^{-1}(X, Y) \cdot \left(\kappa(z'_d(t) - z(t)) - H_{12}(X, \dot{X}, Y, \dot{Y}) \right). \tag{43}$$

where $z'_d(t) = (x_d, \dot{x}_d, y_d, \dot{y}_d, 0, 0, 0, 0)$ in the absence of the bounded internal trajectories and the bounded feedforward input.

Remark 2 It may appear that the same result can be obtained by directly applying stable inversion on the linearized model because the stability in our result is based on linearized system (40) of transformed dynamics (25). Actually, they are different. There are two reasons. First, the desired pair (v_{ff}, z_d) is computed through finding the desired internal (or zero) dynamics of nonlinear unstable system by taking the nonlinear input-output feedback. This desired pair (v_{ff}, z_d) for the nonlinear system can not be obtained via the first approximation of the nonlinear system (21). Second, the linearized model (40) results from the partially feedback linearized (25) where $(z_1, z_2, z_3, z_4) = (x, \dot{x}, y, \dot{y}) \in R^4$ and $(z_5, z_6, z_7, z_8) = (X, \dot{X}, Y, \dot{Y}) \in D_1 \subset R^4$ hold. In comparison, the direct linearized model of the nonlinear system (21) is valid for $(x, \dot{x}, y, \dot{y}) \in D_2 \subset R^4$ and $(X, \dot{X}, Y, \dot{Y}) \in D_3 \subset R^4$. Set D_1, D_2 and D_3 are small sets which contain the origin.

Remark 3 In the last step, we can design some nonlinear stabilizing controller to the partially feedback linearized (25) to enlarge domain of attraction.

Remark 4 Notice the structure of the final control law (42). For each desired trajectory, it is required to compute the corresponding feedforward input and desired state trajectory. Nevertheless, the feedback control law's structure is independent of the particular trajectory to be tracked! Our conclusion is that the stable inversion technique yields a very practical solution to the trajectory tracking problem in this case. Indeed, almost arbitrary trajectories, can be composed of a concatenation of straight lines and circles approximately put together. Using this approach only two set of feedforward control and state have to be computed and a very large set of trajectories may be synthesized.

5 Simulation Studies

The proposed controller (42) is evaluated through computer simulation. The nonlinear model, used as the plant, takes into account some exogenous forces (e.g., viscous friction, input noises) which have been neglected in the design.

Let the exogenous inputs be as follows,

$$v_f = ((-C_x + \Delta_{11})\dot{x} + \Delta_{12}, (-C_y + \Delta_{21})\dot{y} + \Delta_{22}, (-C_X + \Delta_{31})\dot{X}, (-C_Y + \Delta_{41})\dot{Y}) \quad (44)$$

where $\Delta_{ij} \triangleq \sum_{k=1}^M a_{k,ij} \sin(\omega_{k,ij}t + \varphi_{k,ij})$ for $i = 1, 2, 3, 4$ and $j = 1, 2$ with real number $a_{k,ij}$, $\omega_{k,ij}$, $\varphi_{k,ij}$, $k = 1, \dots, M$ are the external disturbances. The root mean square value-RMS of the exogenous disturbances Δ_{ij} for $i = 1, 2, 3, 4$ and $j = 1, 2$ is given by

$$\text{RMS}_{\Delta_{ij}} \triangleq \sqrt{\lim_{T \rightarrow \infty} \frac{1}{T} \int_0^T \Delta_{ij}^2(t) dt} = \sqrt{\frac{1}{2} \sum_{k=1}^M a_{k,ij}^2} \quad (45)$$

The exogenous disturbances (44) together with the proposed control function (42) serve as the generalized input $\{Q\}$ to the plant

$$\{Q\} = (F_x, F_y, 0, 0) + v_f. \quad (46)$$

By the definition (45), we define RMS of the exogenous disturbance at (x, y) direction (i.e., Δ_{12} and Δ_{22}) as follows

$$\text{RMS}_{\Delta_{12,22}} \triangleq \sqrt{\frac{1}{2} \sum_{k=1}^M a_{k,12}^2 + \frac{1}{2} \sum_{k=1}^M a_{k,22}^2} \quad (47)$$

We define RMS of the control signal as follows

$$\text{RMS}_{F_x F_y} \triangleq \sqrt{\frac{1}{T_0} \int_0^{T_0} F_x(t)^2 dt + \frac{1}{T_0} \int_0^{T_0} F_y(t)^2 dt} \quad (48)$$

We define RMS for the translational tracking error $(x_e(t), y_e(t)) \triangleq (x(t) - x_d(t), y(t) - y_d(t))$ as

$$\text{RMS}_{x_e y_e} \triangleq \sqrt{\frac{1}{T_0} \int_0^{T_0} (x(t) - x_d(t))^2 dt + \frac{1}{T_0} \int_0^{T_0} (y(t) - y_d(t))^2 dt} \quad (49)$$

and RMS for the shape tracking error $(X_e(t), Y_e(t)) \triangleq (X(t) - X_d(t), Y(t) - Y_d(t))$ as

$$\text{RMS}_{X_e Y_e} \triangleq \sqrt{\frac{1}{T_0} \int_0^{T_0} (X(t) - X_d(t))^2 dt + \frac{1}{T_0} \int_0^{T_0} (Y(t) - Y_d(t))^2 dt} \quad (50)$$

In the sequel we omit to mention the units for brevity sake. We use for $(x, \dot{x}, y, \dot{y}, X, \dot{X}, Y, \dot{Y})$ the units $(m, m/s, m, m/s, m, m/s, m, m/s)$ respectively. All forces are measured in N (Newtons).

5.1 Finding the Desired States

The desired output profiles (35) and their time derivatives up to second derivative are plotted in Figure 3.

The pair of the desired inputs and the trajectories of internal dynamics found by using iterative procedure (34) are presented in Figure 4 where the desired inputs coincide with the second derivatives of the desired outputs in our case.

5.2 Some Individual Responses

We consider both the effect of friction action and the presence of the exogenous input noise (44).

Case 1: Referring to (45), let RMS for Δ_{i1} with $i = 1, 2, 3, 4$ be $0.01 (N \cdot s/m)$, and RMS for Δ_{i2} with $i = 1, 2$ be $0.02 (N)$. Figure 5(a) shows the signals Δ_{ij} for $i = 1, 2, 3, 4$ and $j = 1, 2$, the exogenous disturbances, which are used in simulations.

The initial condition is

$$(x, \dot{x}, y, \dot{y}, X, \dot{X}, Y, \dot{Y}) = (-1, 0, -1, 0, 0, 0, 0, 0). \quad (51)$$

The simulation results for the nonlinear closed loop system with the controller (42) are shown in Figures 6, 7, 8. From Figure 6, we observe that the outputs (x, y) asymptotically track the desired outputs (x_d, y_d) except for some transient errors (refers to the solid line) immediately after the initial condition and around time 16π (s). Furthermore, the other states asymptotically track their corresponding desired states (see Figure 7) which shows the effectiveness of the stable inversion theory. The transient errors at time 16π (s) arise from that the fact that the given output profiles are not twice differentiable at time 16π (s) (see Figure 8) (This could have been avoided by specifying interpolation conditions using combination of splines to execute this transition. This comes at the cost of calculating off-line a larger set of feedforward strategies.).

Figure 6 shows also the same task using the feedback controller alone (43). It results in larger errors (refers to the dashed line).

Figure 9(a) illustrates how the spherical inverted pendulum with the output tracking controller (42) tracks a moving cursor which represents the specific output profiles. The Figure verifies how natural the controlled pendulum is: at the beginning, the pendulum converges to the cursor very fast; then, the pendulum coincides with the cursor and slightly inclines inward the curvature so as to track the curvature; finally, the cursor suddenly stops at the origin while the pendulum as a physical object can not stop suddenly and overtakes the cursor along the tangent direction of the curvature. Simulation Figure 9(b) illustrates how that the spherical inverted pendulum under feedback control only (43) tracks the moving cursor. Clearly, the exact output tracking strategy improves the tracking performance as compared to feedback control tracking.

Case 2: In this case, we consider larger exogenous inputs. Referring to (45), let RMS for Δ_{i1} with $i = 1, 2, 3, 4$ be $0.05 (N \cdot s/m)$ and RMS for Δ_{i2} with $i = 1, 2$ be $0.1 (N)$. Figure 5(b) shows the signals Δ_{ij} for $i = 1, 2, 3, 4$ and $j = 1, 2$, the exogenous disturbances, which are used in simulations.

To inspect the effect of exogenous disturbances, let the initial condition be

$$(x, \dot{x}, y, \dot{y}, X, \dot{X}, Y, \dot{Y}) = (0, 0, 0, 0, 0, 0, 0, 0). \quad (52)$$

The simulation results are shown in Figures 10, 11. Seeing from Figure 10, we observe that the outputs (x, y) still track the desired outputs (x_d, y_d) well with slightly larger fluctuations than those in *Case 1*. Again, the non-smooth points at the desired output profiles also lead to some transient errors immediately after the initial condition and around time 16π (s) (see Figure 11). Furthermore, the other states show more apparent fluctuations than the outputs (x, y) do (see Figure 10) but the trajectories of those states are still tightly bounded about their desired trajectories. Therefore, it proves that the feedback control part in the controller (42) can reject the disturbance well.

5.3 Control Force Responses

To quantify the robustness through simulations, we consider the system under increasing magnitude exogenous disturbances Δ_{j2} for $j = 1, 2$ with fixed RMS for Δ_{i1} with $i = 1, 2, 3, 4$ be $0.01 (N \cdot s/m)$ and compute RMS of the translational position error $(x_e(t), y_e(t))$, the shape position error $(X_e(t), Y_e(t))$ and the signal to noise ratio $\text{SNR} = 20 \log \left(\frac{\text{RMS}_{F_x F_y}}{\text{RMS}_{\Delta_{12,22}}} \right)$.

The initial condition is (52).

Figure 12(a) shows respectively RMS of (x_e, y_e) response and RMS of (X_e, Y_e) response against RMS of the exogenous disturbance Δ_{12} and Δ_{22} . RMS has been computed over a finite time window $t \in [0, T_0] = [5, 50] (s)$ (corresponding to the ellipse smooth trajectory). The $\text{RMS}_{x_e y_e}$ response and $\text{RMS}_{X_e Y_e}$ response almost grow linearly with respect to $\text{RMS}_{\Delta_{12,22}}$ respectively when $\text{RMS}_{\Delta_{12,22}}$ is not too large, for example, less than $0.9(N)$. In this case, linear gains are approximately $\text{RMS}_{x_e y_e} = 0.75(m/N) \cdot \text{RMS}_{\Delta_{j2}}$ and $\text{RMS}_{X_e Y_e} = 0.046(m/N) \cdot \text{RMS}_{\Delta_{j2}}$. Figure 12(b) shows the control signal to noise ratio (SNR) $20 \log \left(\frac{\text{RMS}_{F_x F_y}}{\text{RMS}_{\Delta_{12,22}}} \right)$ against the noise $\log(\text{RMS}_{\Delta_{12,22}})$. When the disturbance intensity becomes too large, larger than $1.6(N)$, all trajectories wander off as the control forces are unable to overcome the friction force and the external disturbances and the pendulum falls down (in this case, due to the singularity at $\sqrt{X^2 + Y^2} \rightarrow L$, our simulation program stops running in MATLAB!). Given that only a linear feedback strategy was presented in (42), this should not come as a surprise. In future work, we will investigate if it is possible to obtain a semi-global domain of attraction for the tracking strategy using nonlinear feedback control ideas.

5.4 Summary of Simulation Results

We summarize the simulations with the following observations

- 1) the simulations illustrate the effectiveness of the stable inversion theory, in that the closed loop system is able to track a large family of sufficiently smooth trajectories. The domain of attraction is some neighborhood of the derived trajectory (see Figure 6).
- 2) a larger class of trajectories constructed as the piecewise continuous concatenation of smooth trajectories can be tracked with adequate performance, allowing for some transients at the concatenation points where insufficient smoothness is encountered (see Figures 8, 11);
- 3) the tracking performance is reasonably robust with respect to unmodelled forces (see Figure 12(a)).

6 Conclusion

We address the output tracking problem of the spherical inverted pendulum and propose an exact output tracking controller. The exact output tracking controller is derived based on the nonlinear stable inversion technique for some output profiles which are achievable by the technique. The simulation results show that the tracking control through stable inversion technique provides a robust and very practical solution to tracking in the nontrivial underactuated mechanical system. To the best of our knowledge, the controller is the first tracking controller for the nonlinear spherical inverted pendulum in the literature. Our future work is to seek nonlinear feedback control instead of linear feedback control to enlarge the domain of attraction and further improve robustness. Implementation of design issues are also under consideration.

Acknowledgments

This research has been supported by the Centre of Excellence in Guidance and Control, funded by Defence Science & Technology Organization, Australia.

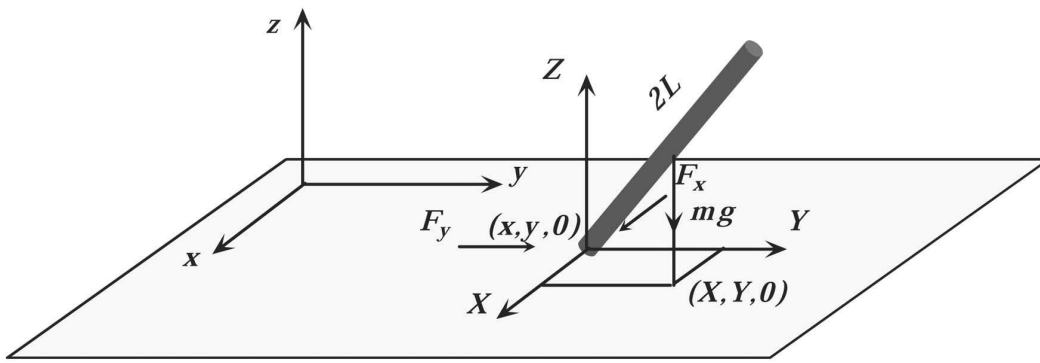


Figure 1. The configuration of the spherical inverted pendulum

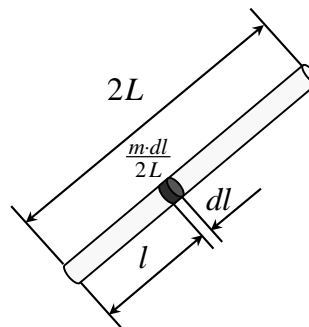


Figure 2. A particle in the spherical inverted pendulum

Appendix A: Entries of Equations (18)

$$\begin{aligned} \ddot{x} = & \frac{4(L^2 + 3Y^2)(F_x + v_{f_1})}{m(L^2 + 3(X^2 + Y^2))} + \frac{-12XY(F_y + v_{f_2})}{m(L^2 + 3(X^2 + Y^2))} \\ & + \frac{-3(L^2 - X^2 + 3Y^2) \left(-\frac{4mX(L^2(\dot{X}^2 + \dot{Y}^2) - (\dot{X}Y - \dot{Y}X)^2)}{3(L^2 - X^2 - Y^2)^2} + \frac{mgX}{\sqrt{L^2 - X^2 - Y^2}} v_{f_3} \right)}{m(L^2 + 3(X^2 + Y^2))} \\ & + \frac{12XY \left(-\frac{4mY(L^2(\dot{X}^2 + \dot{Y}^2) - (\dot{X}Y - \dot{Y}X)^2)}{3(L^2 - X^2 - Y^2)^2} + \frac{mgY}{\sqrt{L^2 - X^2 - Y^2}} v_{f_4} \right)}{m(L^2 + 3(X^2 + Y^2))} \end{aligned}$$

$$\begin{aligned} \ddot{y} = & \frac{-12XY(F_x + v_{f_1})}{m(L^2 + 3(X^2 + Y^2))} + \frac{4(L^2 + 3X^2)(F_y + v_{f_2})}{m(L^2 + 3(X^2 + Y^2))} \\ & + \frac{12XY \left(-\frac{4mX(L^2(\dot{X}^2 + \dot{Y}^2) - (\dot{X}Y - \dot{Y}X)^2)}{3(L^2 - X^2 - Y^2)^2} + \frac{mgX}{\sqrt{L^2 - X^2 - Y^2}} v_{f_3} \right)}{m(L^2 + 3(X^2 + Y^2))} \\ & + \frac{-3(L^2 + 3X^2 - Y^2) \left(-\frac{4mY(L^2(\dot{X}^2 + \dot{Y}^2) - (\dot{X}Y - \dot{Y}X)^2)}{3(L^2 - X^2 - Y^2)^2} + \frac{mgY}{\sqrt{L^2 - X^2 - Y^2}} v_{f_4} \right)}{m(L^2 + 3(X^2 + Y^2))} \end{aligned}$$

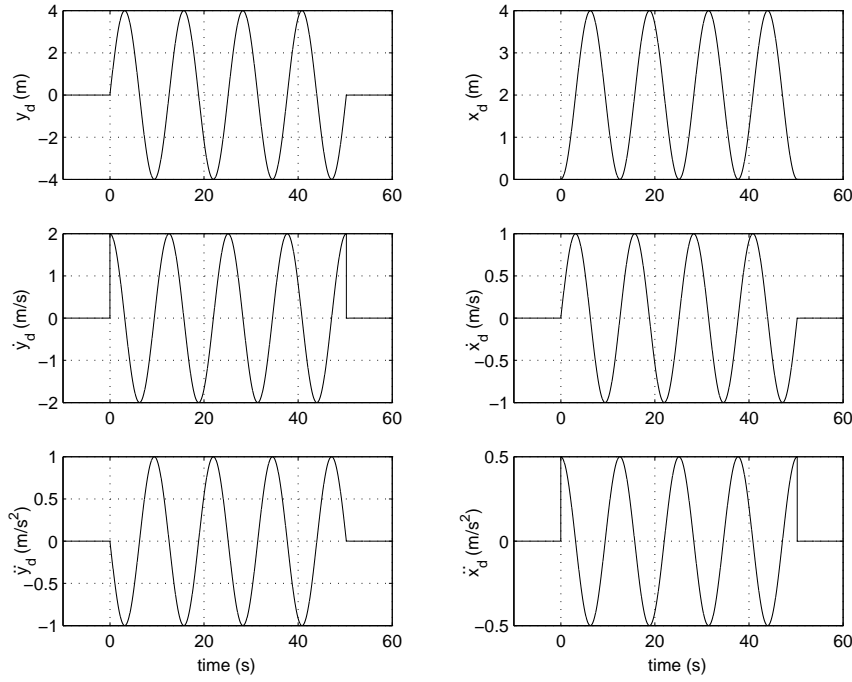


Figure 3. The desired output profiles and their time derivatives

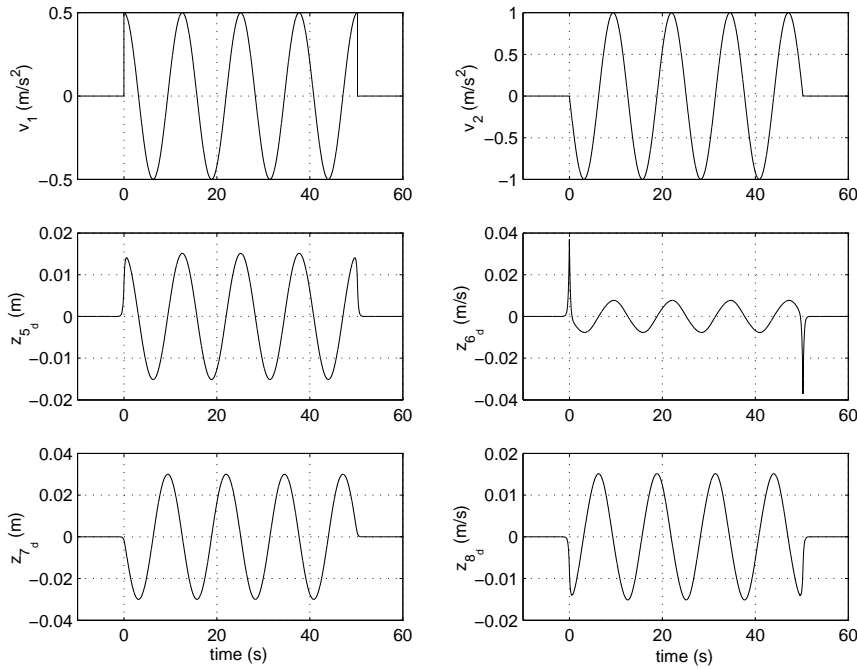


Figure 4. The pair of the desired input and the desired trajectories of internal dynamics

$$\begin{aligned}
 \ddot{X} = & \frac{-3(L^2 - X^2 + 3Y^2)(F_x + v_{f_1})}{m(L^2 + 3(X^2 + Y^2))} + \frac{12XY(F_y + v_{f_2})}{m(L^2 + 3(X^2 + Y^2))} \\
 & + \frac{3(L^2 - X^2 + 3Y^2) \left(-\frac{4mX(L^2(\dot{X}^2 + \dot{Y}^2) - (\dot{X}Y - \dot{Y}X)^2)}{3(L^2 - X^2 - Y^2)^2} + \frac{mgX}{\sqrt{L^2 - X^2 - Y^2}} v_{f_3} \right)}{m(L^2 + 3(X^2 + Y^2))} \\
 & + \frac{-12XY \left(-\frac{4mY(L^2(\dot{X}^2 + \dot{Y}^2) - (\dot{X}Y - \dot{Y}X)^2)}{3(L^2 - X^2 - Y^2)^2} + \frac{mgY}{\sqrt{L^2 - X^2 - Y^2}} v_{f_4} \right)}{m(L^2 + 3(X^2 + Y^2))}
 \end{aligned}$$

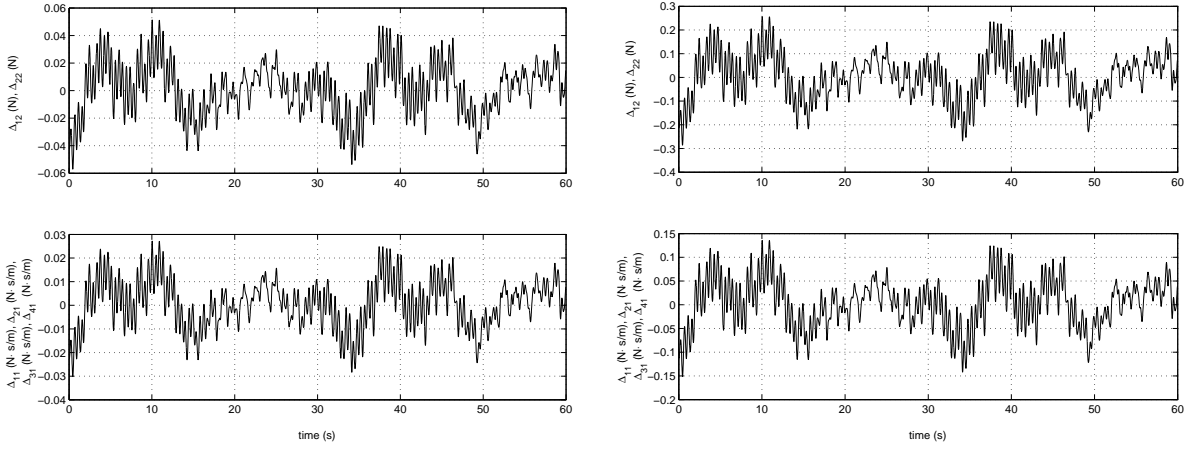
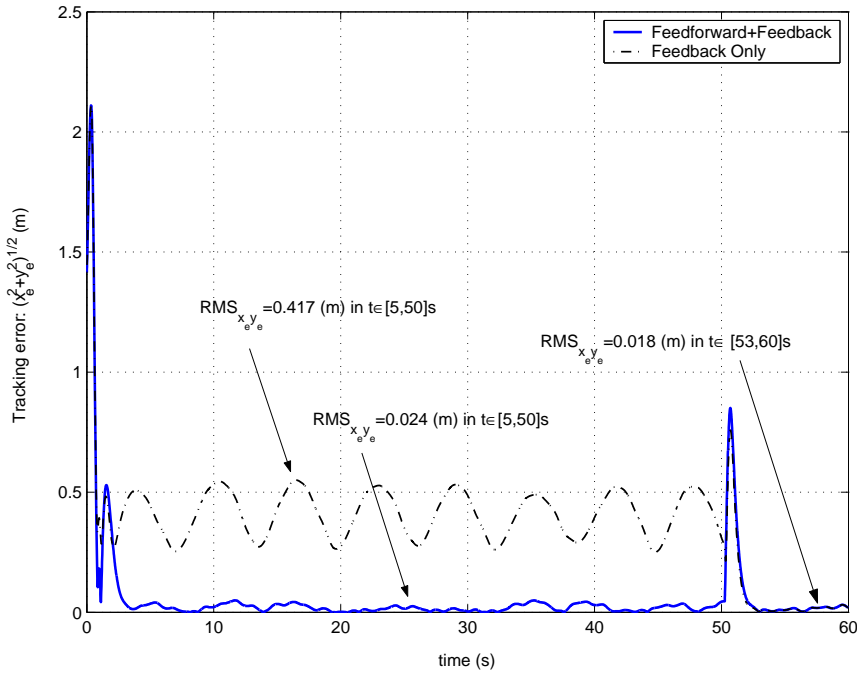
(a) Noise model in *Case 1*(b) Noise model in *Case 2*

Figure 5. Friction and exogenous disturbances

Figure 6. Output tracking errors in *Case 1*

$$\begin{aligned} \ddot{Y} = & \frac{12XY(F_x + v_{f1})}{m(L^2 + 3(X^2 + Y^2))} + \frac{-3(L^2 + 3X^2 - Y^2)(F_y + v_{f2})}{m(L^2 + 3(X^2 + Y^2))} \\ & + \frac{-12XY \left(-\frac{4mX(L^2(\dot{X}^2 + \dot{Y}^2) - (\dot{X}Y - \dot{Y}X)^2)}{3(L^2 - X^2 - Y^2)^2} + \frac{mgX}{\sqrt{L^2 - X^2 - Y^2}} v_{f3} \right)}{m(L^2 + 3(X^2 + Y^2))} \\ & + \frac{3(L^2 + 3X^2 - Y^2) \left(-\frac{4mY(L^2(\dot{X}^2 + \dot{Y}^2) - (\dot{X}Y - \dot{Y}X)^2)}{3(L^2 - X^2 - Y^2)^2} + \frac{mgY}{\sqrt{L^2 - X^2 - Y^2}} v_{f4} \right)}{m(L^2 + 3(X^2 + Y^2))} \end{aligned}$$

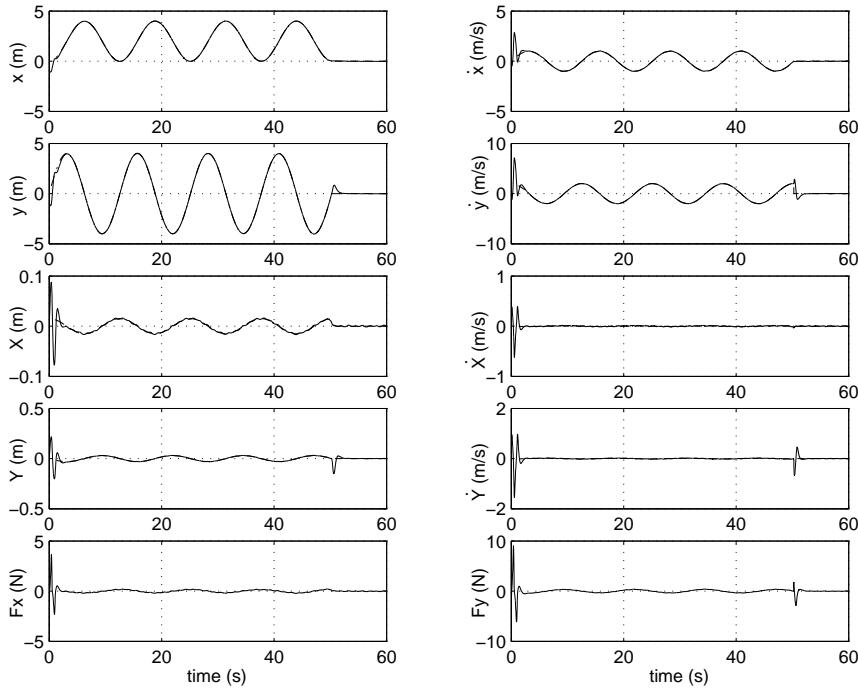


Figure 7. State trajectories ‘-’ and their references ‘.-’ in *Case 1*

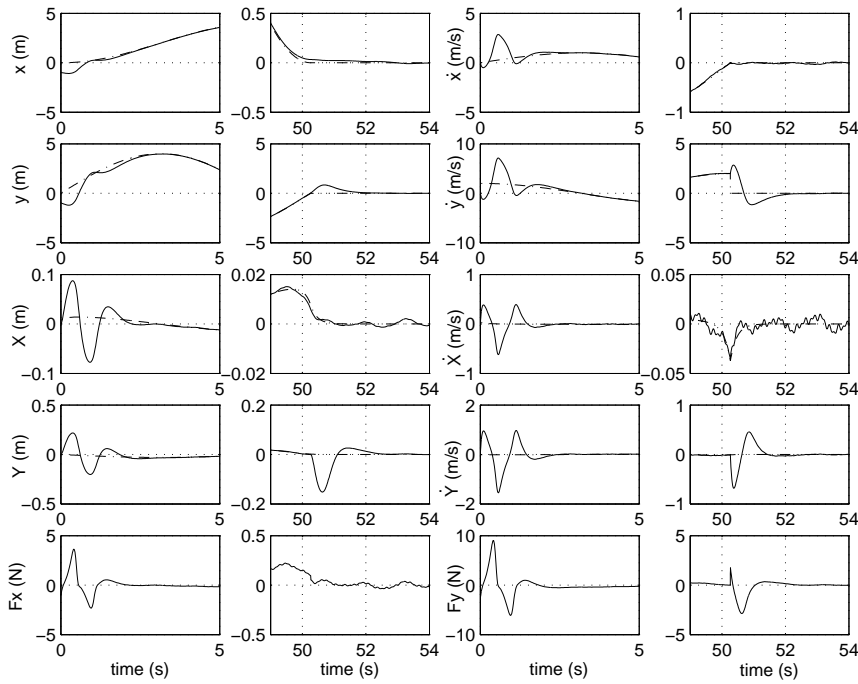
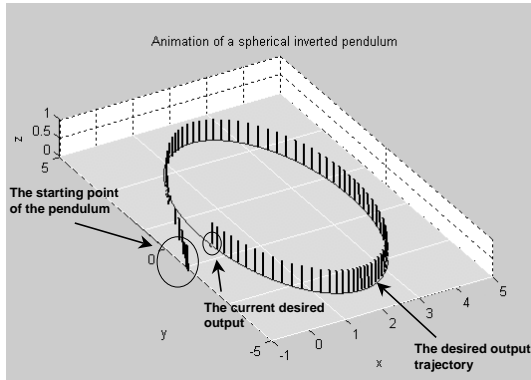


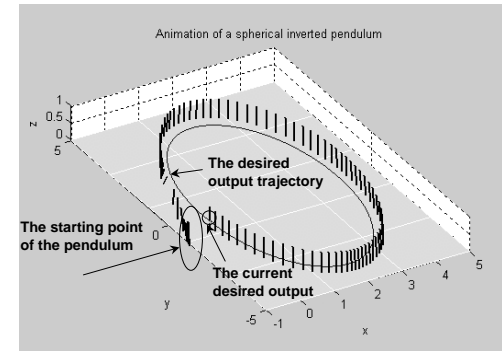
Figure 8. Transient errors with state trajectories ‘-’ and their references ‘.-’ in *Case 1*

Appendix B: Entries of $H_{11}(X, Y)$, $H_{12}(X, Y)$, $H_{21}(X, \dot{X}, Y, \dot{Y})$, $H_{22}(X, \dot{X}, Y, \dot{Y})$

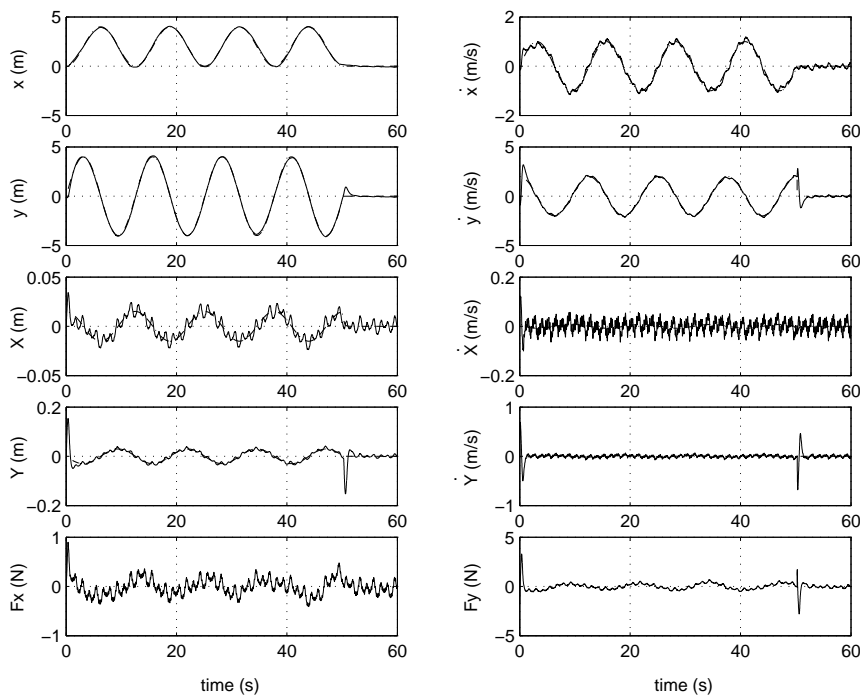
$$H_{11}(X, Y) = \begin{pmatrix} \frac{4(L^2+3Y^2)}{m(L^2+3(X^2+Y^2))} & \frac{-12XY}{m(L^2+3(X^2+Y^2))} \\ \frac{-12XY}{m(L^2+3(X^2+Y^2))} & \frac{4(L^2+3X^2)}{m(L^2+3(X^2+Y^2))} \end{pmatrix}, H_{21}(X, Y) = \begin{pmatrix} \frac{-3(L^2-X^2+3Y^2)}{m(L^2+3(X^2+Y^2))} & \frac{12XY}{m(L^2+3(X^2+Y^2))} \\ \frac{12XY}{m(L^2+3(X^2+Y^2))} & \frac{-3(L^2+3X^2-Y^2)}{m(L^2+3(X^2+Y^2))} \end{pmatrix},$$



(a) Illustration of the exact output tracking



(b) Illustration of the feedback control only

Figure 9. Comparison of the performance in *Case 1*Figure 10. State trajectories '·' and their references '·' in *Case 2*

Because $\det(H_{11}(X, Y)) = 16L^2(L^2 + 3y^2 + 3x^2) > 0$ hold for any $(X, Y) \in U$, $H_{11}(X, Y)$ is invertible on U .

$$H_{12}(X, \dot{X}, Y, \dot{Y}) = \begin{pmatrix} \frac{12XY \left(-\frac{4mY(L^2(\dot{X}^2 + \dot{Y}^2) - (\dot{X}Y - \dot{Y}X)^2)}{3(L^2 - X^2 - Y^2)^2} \right) - 3(L^2 - X^2 + 3Y^2) \left(-\frac{4mX(L^2(\dot{X}^2 + \dot{Y}^2) - (\dot{X}Y - \dot{Y}X)^2)}{3(L^2 - X^2 - Y^2)^2} \right)}{m(L^2 + 3(X^2 + Y^2))} \\ \frac{12XY \left(-\frac{4mX(L^2(\dot{X}^2 + \dot{Y}^2) - (\dot{X}Y - \dot{Y}X)^2)}{3(L^2 - X^2 - Y^2)^2} \right) - 3(L^2 + 3X^2 - Y^2) \left(-\frac{4mY(L^2(\dot{X}^2 + \dot{Y}^2) - (\dot{X}Y - \dot{Y}X)^2)}{3(L^2 - X^2 - Y^2)^2} \right)}{m(L^2 + 3(X^2 + Y^2))} \end{pmatrix},$$

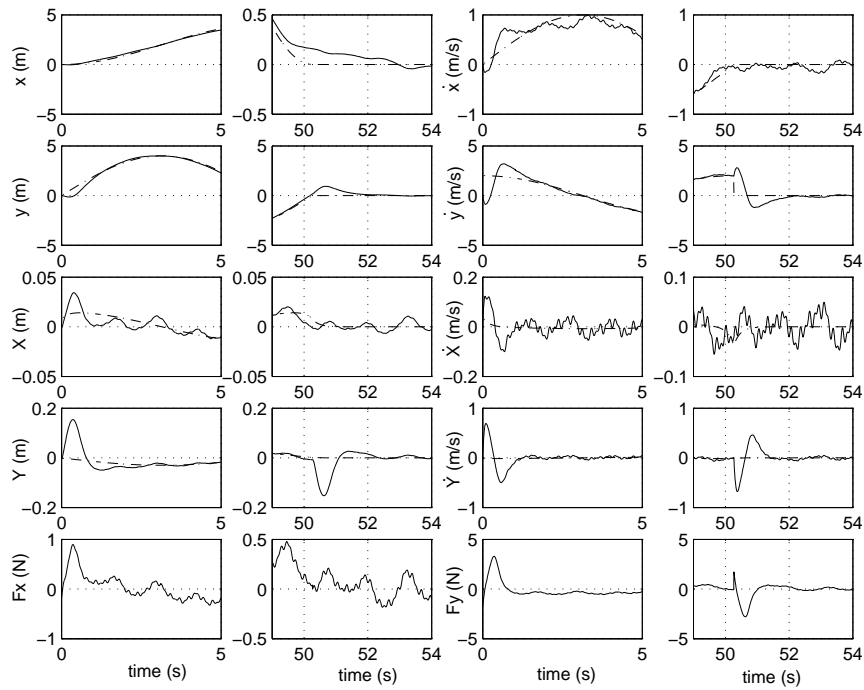
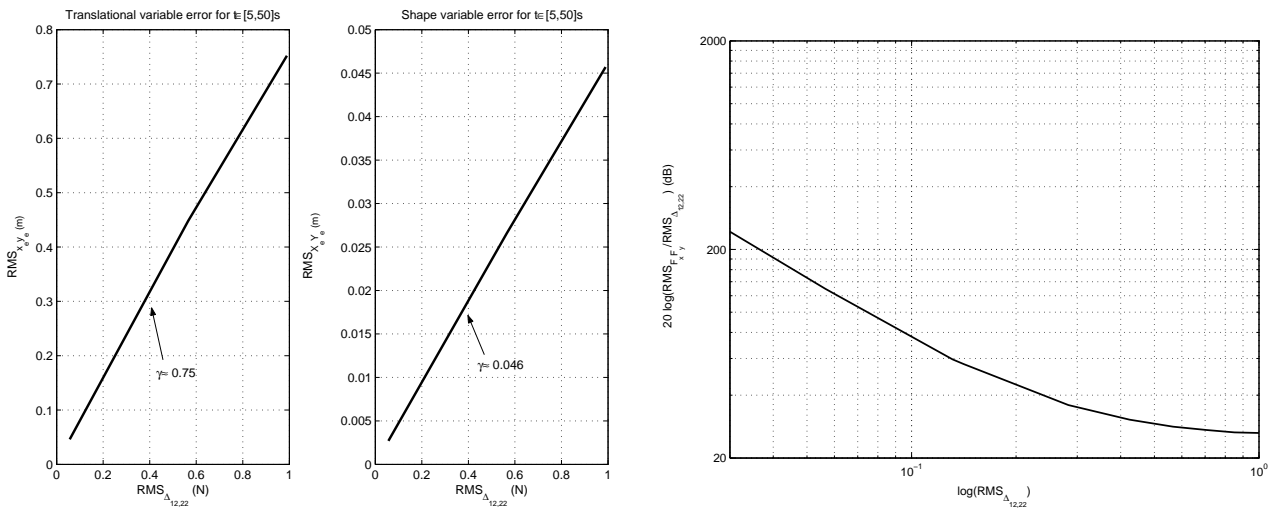


Figure 11. Transient errors with state trajectories ‘-’ and their references ‘.-’ in Case 2



(a) The impact of exogenous noises upon the performance

(b) Control signal to noise ratio (SNR) against the noise

Figure 12. Evaluation of the robustness

$$H_{22}(X, \dot{X}, Y, \dot{Y}) = \begin{pmatrix} \frac{3(L^2 - X^2 + 3Y^2) \left(-\frac{4mX(L^2(\dot{X}^2 + \dot{Y}^2) - (\dot{X}Y - \dot{Y}X)^2)}{3(L^2 - X^2 - Y^2)^2} \right) - 12XY \left(-\frac{4mY(L^2(\dot{X}^2 + \dot{Y}^2) - (\dot{X}Y - \dot{Y}X)^2)}{3(L^2 - X^2 - Y^2)^2} \right)}{m(L^2 + 3(X^2 + Y^2))} \\ \frac{3(L^2 + 3X^2 - Y^2) \left(-\frac{4mY(L^2(\dot{X}^2 + \dot{Y}^2) - (\dot{X}Y - \dot{Y}X)^2)}{3(L^2 - X^2 - Y^2)^2} \right) - 12XY \left(-\frac{4mX(L^2(\dot{X}^2 + \dot{Y}^2) - (\dot{X}Y - \dot{Y}X)^2)}{3(L^2 - X^2 - Y^2)^2} \right)}{m(L^2 + 3(X^2 + Y^2))} \end{pmatrix}$$

References

- A. Bloch, N. Leonard, and J. Marsden, "Controlled lagragians and the stabilisation of mechanical systems i: the first matching theorem," *IEEE Transactions on Automatic Control*, vol. 45, pp. 2253–2269, 2000.
- A. Bloch, D. Chang, N. Leonard, and J. Marsden, "Controlled lagragians and the stabilisation of mechanical systems ii: potential shaping," *IEEE Transactions on Automatic Control*, vol. 46, pp. 1556–1571, 2001.
- D. Croft, D. Shedd, and S. Devasia, "Creep, hysteresis, and vibration compensation for piezoactuators: atomic force microscopy application," *ASME Journal of Dynamics Systems, Measurement and Control*, vol. 123, pp. 35–43, 2001.
- S. Devasia, "Approximated stable inversion for nonlinear systems with nonhyperbolic internal dynamics," *IEEE Transactions on Automatic Control*, vol. 44, pp. 1419–1425, 1999.
- S. Devasia, "Should model-based inverse inputs be used as feedforward under plant uncertainty?" *IEEE Transactions on Automatic Control*, vol. 47, pp. 1865–1871, 2002.
- S. Devasia, D. Chen, and B. Paden, "Nonlinear inversion-based output tracking," *IEEE Transactions on Automatic Control*, vol. 41, pp. 930–942, 1996.
- J. Dewey, K. Leang, and S. Devasia, "Experimental and theoretical results in output-trajectory redesign for flexible structures," *ASME Journal of Dynamic Systems, Measurement, and Control*, vol. 120, pp. 456–461, 1998.
- R. Hirschorn, "Invertibility of multivariable nonlinear control system," *IEEE Transactions on Automatic Control*, vol. 6, pp. 855–865, 1979.
- L. Hunt, G. Meyer, and R. Su, "Noncausal inverses for linear systems" *IEEE Transactions on Automatic Control*, vol. 41, pp. 608–611, 1996.
- A. Isidori, *Nonlinear Control System (3rd edition)*. Springer, 1995.
- G. Liu, D. Nešić, and I. Mareels, "Modelling and stabilisation of a spherical inverted pendulum," in *Proceeding of IFAC*, Prague, Czech Republic, 2005.
- , "Non-local Stabilization of a Spherical Inverted Pendulum," Submitted to International Journal of Control.
- R. Olfati-Saber "Nonlinear Control of Underactuated Mechanical Systems with Application to Robotics and Aerospace Vehicles," *Ph.D Thesis, Massachusetts Institute of Technology*, 2001.
- J. Slotine and W. Li, *Applied Nonlinear Control*. Prentice Hall, 1991.
- A. Teel, "A nonlinear small gain theorem for the analysis of control systems with saturation," *IEEE Transactions on Automatic Control*, vol. 41, pp. 1256–1270, 1996.
- W. Yim and S. Singh, "Nonlinear inverse and predictive end point trajectory control of flexible macro-micro manipulators," *Journal of Dynamics Systems, Measurement and Control*, vol. 119, pp. 412–420, 1997.
- Q. Zou and S. Devasia, "Preview-based inversion of nonlinear nonminimum-phase systems: Vtol example," in *Proc. of IEEE conference on Decision and Control*, Paradise Island, Bahamas, USA, 2004, pp. 4350–4356.